Published in final edited form as:
Parasitol Int. 2010 December ; 59(4): 565–570. doi:10.1016/j.parint.2010.07.007.

High-content imaging for automated determination of host-cell infection rate by the intracellular parasite *Trypanosoma cruzi*

L.L. Nohara[1], **C. Lema**[1,2], **J.O. Bader**[3], **R.J. Aguilera**[1,2], and **I.C. Almeida**[1,*]

[1]The Border Biomedical Research Center, Department of Biological Sciences, University of Texas at El Paso, El Paso, Texas

[2]Cell Culture and High-Throughput Screening Core Facility, The Border Biomedical Research Center, Department of Biological Sciences, University of Texas at El Paso, El Paso, Texas

[3]Statistical Consulting Laboratory, The Border Biomedical Research Center, University of Texas at El Paso, El Paso, Texas

Abstract

Chagas disease affects 8–11 million people, mostly in Latin America. Sequelae include cardiac, peripheral nervous and/or gastrointestinal disorders, thus placing a large economic and social burden on endemic countries. The pathogenesis and the evolutive pattern of the disease are not fully clarified. Moreover, available drugs are partially effective and toxic, and there is no vaccine. Therefore, there is an urgent need to speed up basic and translational research in the field. Here, we applied automated high-content imaging to generate multiparametric data on a cell-by-cell basis to precisely and quickly determine several parameters associated with *in vitro* infection of host-cell by *Trypanosoma cruzi*, the causative agent of Chagas disease. Automated and manual quantification was used to determine the percentage of *T. cruzi*-infected cells in a 96-well microplate format and the data generated was statistically evaluated. Most importantly, this automated approach can be widely applied for discovery of potential drugs as well as molecular pathway elucidation not only in *T. cruzi* but also other human intracellular pathogens.

Keywords

Chagas disease; Host-cell infection rate; High-content imaging; Intracellular parasite; *Trypanosoma cruzi*

1. Introduction

The year 2009 marked the 100th anniversary of the discovery of Chagas disease and its causative agent, *Trypanosoma cruzi*, by the Brazilian physician Carlos R.J. Chagas while he was working at the Oswaldo Cruz Institute in Rio de Janeiro [1]. The impact of Chagas disease, once thought to be limited to Latin America, where an estimated 8 to 11 million people are chronically infected, has moved to the United States and Europe, mainly due to migration from

[*]**Corresponding author.** University of Texas at El Paso, Department of Biological Sciences, The Border Biomedical Research Center, 500 W University Avenue, El Paso, TX, 79968-0519; Tel.: (915) 747 6086; Fax: (915) 747 5808; icalmeida@utep.edu.

endemic areas of Mexico, Central America, and South America [2]. The estimated number of infected persons living in the United States is 300,000 or more, based on estimated disease rates by country of origin [3]. Furthermore, the parasite can be found in reduviid bugs and mammals in the southern regions of the United States [4–6], and there have been a few reported cases of autochthonous, and transplant- and blood donation-related transmissions in humans [7–9].

Many aspects of Chagas disease pathogenesis are still not well understood. The current drug treatment regimens for the established chronic phase of the infection are partially effective and highly toxic [10–12], and acute disease reactivation can occur due to immunosuppression [13]. In addition, development of chemotherapy resistance has been reported [14]. Therefore, there is an urgent need to develop effective chemotherapeutics and/or vaccine against Chagas disease, which is the most significant parasitic infection of the Americas [12].

T. cruzi is an intracellular protozoan parasite and its ability to infect and replicate within a cell is an essential feature for completion of its life cycle in the mammalian host-cell. Upon host-cell infection, the infective *T. cruzi* trypomastigote forms differentiate into replicative amastigote forms and begin to divide. Then, amastigotes differentiate back into trypomastigotes, the host-cell ruptures releasing the parasites into the extracellular milieu where they can infect adjacent cells and go to the bloodstream to infect other tissues, or be ingested by a reduviid insect vector [15].

To gain insights into the molecular mechanisms that regulate *T. cruzi* host-cell invasion, intracellular proliferation and other events during parasite-host cell interactions as well as for identification of compounds with anti-parasitic effects, studies based on *in vitro T. cruzi* infection have largely relied on the application of labor-intensive manual counting of host cells and parasites by light or fluorescence microscopy. Typically, these assays are performed in individual coverslips and parasites are detected by Giemsa staining [16,17], DNA is labeled with fluorescent dyes or by immunostaining using anti-*T. cruzi* antibodies followed by a fluorescent secondary antibody [18,19]. The analysis then involves the visual counting of intracellular parasites in each of the one hundred to five hundred cells per sample. In addition, compounds against *T. cruzi* have been evaluated by manually counting the parasites released into the supernatant of infected cells and by assays using extracellular parasites [20]. These methods based on visual scoring and manual annotation are time-consuming, potentially biased by the operator, and unsuitable for the analysis of larger number of biological samples.

To date, only few reports have tried to address these concerns. Buckner et al. (1996) engineered parasites expressing β-galactosidase for colorimetric assays [21]. Alternatively, an assay based on the selective incorporation of radioactive uracil by parasite-infected cells has been described [22]. More recently, Hyland et al. (2008) engineered *T. cruzi* expressing firefly luciferase for bioluminescent determination of infection rates [23], These approaches have been applied for screening of compounds against *T. cruzi* [24,25]. However, in addition to other disadvantages, these methods require separate assays for assessment of mammalian cell toxicity and the results are an average of the biological responses of thousands of cells.

Conversely, current new technologies offer numerous advantages when compared to conventional procedures. The recent emergence of high-content imaging, which is based on automated fluorescence image acquisition, processing and analysis, has provided unique and powerful tools to quantitatively determine spatiotemporal events in complex biological systems [26]. This technology is based on single-cell analysis in large cell populations allowing precise, efficient and simultaneous assessment of multiple cellular parameters relevant for evaluating the potential of novel compounds and dissecting signaling pathways. Recent reports have confirmed the potential of image-based cellular screening to monitor and quantify several

cellular events such as protein nuclear translocation [27,28], G-protein coupled receptor activity [29], microtubule dynamics [30] in addition to aid in the identification of compounds that interfere with these biological processes. High-content imaging has also been successfully applied for screening of RNA interference libraries [31] and identification of host kinases and respective inhibitors that prevent bacterial intracellular growth [32]. Recently, this approach has been applied for the in vitro drug screening of anti-*T. cruzi* compounds [33]; however, the accuracy of the procedure in regard to the manual parasite counting method has not yet been evaluated.

In the present report, we evaluate a high-content imaging method for automated quantification of host-cell infection rate by the intracellular parasite *T. cruzi*. The ability of this technology to perform quantitative assessment of multiple cellular parameters on a cell-by-cell basis in a multiwell plate format, makes it especially attractive not only for high-throughput screening of potential anti-parasitic drugs but also for studying parasite molecular pathways. Here, the number of parasites per 100 cells and percentage of infected cells were determined both by conventional manual counting (manual method) and automated high-content imaging analysis (automated method), and the data was statistically compared.

2. Materials and Methods

2.1. Parasites and mammalian cell culture

Murine NIH 3T3 fibroblasts (ATCC, Manassas, VA), were cultured in Dulbecco's modified Eagle's medium (DMEM) supplemented with 10% bovine calf serum (BCS) (DMEM-BCS) at 37°C in a 5% CO_2 humidified atmosphere. Tissue culture-derived *T. cruzi* trypomastigote forms (Y strain) were obtained from the supernatant of infected LLC-MK2 (Rhesus monkey kidney epithelial cells; ATCC, Manassas, VA), 5 to 9 days post-infection by weekly passages [34]. Cell cultures were regularly tested for *Mycoplasma* by polymerase chain reaction (PCR) [35].

2.2. Generation of green fluorescence protein (GFP) expressing NIH 3T3 cells

To generate GFP-expressing NIH 3T3 cultures, cells were transfected with the psi-h7SKGFPzeo-derived silencing vector encoding a hairpin specifically targeting LacZ (InvivoGen, San Diego, CA) by nucleofection using the Cell Line Nucleofector Kit R (Lonza, Walkersville, Inc., MD). As the vector contains a GFP reporter gene combined with the Zeocin resistance gene, stable transfectants were selected in medium containing Zeocin (InvivoGen, San Diego, CA). The successful selection of the transfectants was confirmed by analyzing the percentage of cells expressing GFP using flow cytometry.

2.3. Infection assays

For the *in vitro* infection assay GFP-expressing NIH 3T3 cells were plated onto BD Falcon 96-well bioimaging plates (BD Biosciences, Rockville, MD), at a density of 4×10^3 cells per well, and incubated overnight at 37°C in a 5% CO_2 humidified atmosphere. Before infection, cells were washed once with complete medium (DMEM-BCS) to remove nonadhered cells. Trypomastigotes were added at a parasite:host cell ratio of 5:1 and infections were carried out for 2 h at 37°C in a 5% CO_2 humidified atmosphere. After incubation, cells were washed four times with phosphate-buffered saline (PBS), pH 7.4,, and reincubated with DMEM-BCS for approximately 18 h to allow the differentiation of internalized parasites into amastigote forms, which are more easily quantified than intracellular trypomastigotes. In line with previous observations [36–38], in our model replication is observed at later time points ensuring that parasite counting represents infection rather than replication rate. Cells were washed with PBS and fixed with 4% paraformaldehyde for 15 min at room temperature. Parasite and host-cell

DNA were subsequently stained with 4',6-diamidino-2-phenylindole (DAPI) (Sigma Aldrich) at 1 μg/mL for 5 min and washed with PBS.

2.4. Image acquisition, processing, and analysis

Image acquisition and analysis of microplates were carried out using the BD Pathway 855 high-resolution fluorescence bioimager system (BD Biosciences). Filter sets appropriate for the excitation and emission spectra of GFP and DAPI were selected. Images from nine contiguous image fields (3 × 3 montage) were acquired per well with a 20× (0.75 numerical aperture, NA) objective. For optimal segmentation and counting of parasites associated with host-cells, the BD AttoVision™ v1.6.2 Sub Object analysis was applied. This software tool provides comprehensive measurement of parameters for counting spots (intracellular parasites) within a boundary object (host cell), enabling their accurate quantification. GFP was used to define the boundary object (host-cell body); whereas DAPI was used to define the counting spots (intracellular parasites). Although the parasite DNA staining with DAPI may result in a doublet due to the presence of genomic and kinetoplastid DNA, images were acquired using a 20× (0.75 NA) objective to obtain higher cell counts per field for a statistically representative data set. At this optical resolution, genomic and kinetoplastid DNA are not distinguished as separate entities but captured as a single spot. Host-cell nuclei, being much larger than the parasites, were systematically excluded from the analysis, based on their size. Numerical data was imported into the Microsoft Excel-based BD™ Image Data Explorer (BD Biosciences, Rockville, MD) to determine the parameters associated with host-cell infection by *T. cruzi*.

2.5. Statistical analysis

Statistical analysis (Statistical Analysis System, SAS v.9.2 software, SAS Institute, Inc., Cary, NC) was applied to compare the data generated by manual and automated counting methods. A set of 21 treatment groups from an on-going study were used to compare manual and automated assessment of the following two parameters: (i) number of intracellular parasites per 100 cells and (ii) the percentage of infected cells. For each treatment group, 3–4 replicates were available, rendering a total of 77 data points for analysis. Manual and automated methods were compared using the paired-sample t-test for testing whether the mean of the absolute difference or the mean of the percent absolute difference (with manual counting as base) both differed from 0 for each parameter evaluated. Briefly, for each data point we had a couple of values, one generated by the manual method and the other derived from the automated method. Subtraction of one value from the other renders the absolute difference of each couple of values. The mean of the absolute difference is calculated by adding up all the absolute difference values and diving them by the number of data points (n=77). If the value derived from the manual method is taken as 100% and the value generated by the automated method is expressed as the percent of the manual method, their subtraction renders the percent absolute difference of each couple of values. This time, the mean of the percent absolute difference is calculated by adding up all the percent absolute difference values and diving them by the number of data points (n=77). Along with each mean value, its respective standard deviation (SD) was obtained.

Also, a simple linear regression model was fitted to the data, the slope of the line tested against 1 and the y-intercept tested against 0 using t-tests. Finally, the General Linear Mixed Model analysis for repeated measures was applied to compare the mean values obtained by the manual and automated methods for both parameters across the 21 treatment groups. All tests were conducted at the 0.05 level of significance (p-value).

3. Results and Discussion

As with any high-content assay, numerous parameters including adaptation to multiwell microplates, image acquisition, and image analysis were optimized during the development of

the assay. A general workflow of the high-content imaging process applied for automated quantification of host-cell infection rate by the intracellular parasite *T. cruzi* is shown in Figure 1. The method includes 4 steps: plate set up, image capture, image analysis, and data analysis. After the establishment of the biological model for *in vitro* infection of GFP-expressing NIH 3T3 cells with *T. cruzi* trypomastigotes in a 96-well plate format, cells were seeded, infected, fixed and subsequently stained with DAPI. In order to determine the number of parasites within a single host cell, GFP fluorescence was used to define the host-cell boundaries, whereas DAPI staining provided the total number of host cells and parasites. In order to obtain statistically representative data, capture of a large enough population of host cells per image was needed. To accomplish this task, nine contiguous image fields (3 × 3 montage) were acquired to obtain a single montage image. We then combined several image pre-processing and segmentation tools in order to optimize the image analysis protocol, which enabled specific host-cell and parasite segmentation as verified by visual inspection of the images. Briefly, segmentation consists of the application of intensity thresholds to define cellular regions (also called regions of interest or ROIs), where measurements will be made. Finally, data was analyzed by applying specific parameter constraints in order to obtain the following parameters: i) total numbers of cells and parasites per well, ii) number of parasites per cell, and iii) percentage of infected cells per well. In our model, we used GFP expressing NIH 3T3 cells, although the same workflow described above should be applicable when using a different cell line, which not necessarily need to express GFP but be stained with a whole cell or plasma membrane dye. However, the latter alternative will also add an extra step during the plate preparation.

Figure 2 shows representative segmented images of the host-cell body (boundary object), host-cell nuclei, and intracellular parasites (sub-object counting spots). Host-cells were properly segmented based on whole-cell GFP expression and DAPI-stained individual nuclei. Although parasites were also stained with DAPI, they were specifically selected by setting a small size threshold that excluded cell nuclei from all counts. The generation of multiparametric data based on single cell information allowed us to determine several parameters linked to host-cell infection by *T. cruzi* in a highly accurate and rapid manner. The number of parasites per hundred cells was obtained through the results of the sub-object analysis, while the percentage of infected cells was determined by applying a data constraint to assess the number of host cells (objects) containing at least one parasite (sub-object).

Overall, the values generated by the manual method were slightly higher than those obtained by the automated quantification. A summary of the statistics for the absolute difference and the percent absolute difference between the manual and automated methods is given in Table 1. Both the mean of the absolute difference and the mean of the percent absolute difference were significantly different from 0 ($p < 0.05$), by the paired sample t-tests. However, for both parameters, the mean of the absolute difference was quite small (2.5 SD±1.5 and 1.7 SD±1.0) for the number of parasites per 100 cells and percentage of infected cells, respectively. Likewise, the mean of the percent absolute difference was 15.4 SD±6.3 and 13.6 SD±6.3 for number of parasites per 100 cells and percent of infected cells, respectively. The scatter plots of manual versus automated values of number of parasites per 100 cells and percentage of infected cells are given in Figure 3. For both parameters, the scatter about the fitted regression line was quite small, so there was a strong linear relationship between the two methods. In fact, the estimated correlation coefficients for number of parasites per 100 cells and percent of infected cells were 0.97 and 0.96, respectively. However, the slope of the line was significantly different from 1 ($p < 0.05$), although the y-intercept was not significantly different from 0 ($p > 0.1$). Again, these results reflect the slightly increased values generated by the manual method as compared to the automated procedure. When the number of parasites per 100 cells was evaluated, the data showed that the manual values were consistently higher than the automated values, by about 0.2230, the y-intercept of the estimated regression line. Likewise, when the percentage of infected cells was evaluated, the data showed the same tendency, i.e., the manual

values were consistently higher than the automated values, by about 0.6229, the y-intercept of the estimated regression line. The estimated slopes for the number of parasites per 100 cells and the percentage of infected cells were 1.1691 and 1.1000, respectively.

The results of the General Linear Mixed Model analysis for repeated measures indicate differences in the means of the two methods across the treatment groups (Figure 4). As expected, we also observed the same trend of higher means for manual method compared to automated method across all of the 21 treatment groups. Despite the observed difference, data showed a linear relationship between the two methods and except for groups 3 and 10, the differences between the manual and automated methods appear not only small but, more importantly, similar. Therefore, if it is the relative change in infection in response to treatment what matters, and not the absolute change, the automated method would prove useful and advantageous. However, given a small difference between treatments groups, it may not prove sensitive enough to ensure detection.

There appear to be two main factors responsible for the slight discrepancy between the manual and automated methods. First, parasites localized immediately next to the host-cell nuclei are frequently not identified as individual entities but part of the host-nuclei and, therefore, undercounted. Second, sub-optimal segmentation for parasites may result from low DAPI fluorescence intensity. To overcome this limitation, parasite surface immunostaining seems a viable option. However, we have observed that given two contiguous parasites, DNA staining rather than surface staining works more effectively to separate them as individual entities, due to the fact that the distance between the nuclei is greater than the distance between the parasite surfaces (data not shown). We have recently applied this automated approach to evaluate the effects of candidate anti-parasite compounds on *T. cruzi* intracellular proliferation (Nohara et al., unpublished). Our results further confirmed the applicability of automated counting even in experimental settings where more than 100 parasites are found inside of an infected cell (data not shown).

The most significant advantage of the automated method over the manual counting is that it reduces dramatically the sample processing time as it is illustrated in Table 2. Visual assessment of the percentage of infected cells and the number of parasites per 100 cells for a single sample takes approximately 1 h. Thus, the estimated time needed to manually process a 96-well plate, will be 96 h or 12 working days (8 h each). The automated method will accomplish the same task in 14 h or about 2 working days. This means an increase of sample processing speed of about 6 times. In addition, operator's exhaustion is not an issue for the automated method, where only few hours of operator's working day are required to set the parameters of each automated processing step, whereas manual counting is tiring and requires the operator's physical presence during the whole process.

Since the automated analysis is based on the determination of sub-objects (parasites) within the boundaries of the object (host cell), membrane-bound extracellular parasites can be miscounted as intracellular parasites. This limitation however, is valid not only for the automated approach but also for the conventional manual counting. To solve this issue, differential detection of extracellular parasites may be achieved by carrying out parasite-specific immunofluorescence labeling in nonpermeabilized cells, which will result in additional steps during sample preparation as well as longer time periods required for image acquisition, processing, and data analysis.

Conclusion

In contrast to manual counting, automated high-content imaging is highly objective, accurate, and significantly faster, being based on automated digital microscopy coupled with computer-

based data analysis. The images clearly show the feasibility of documenting and quantitatively analyzing not only the degree of *T. cruzi* infection but also the level of parasite intracellular proliferation using this method. Additionally, when the methodology is applied for the study of compounds effects on the parasite infectivity or proliferation, the response of mammalian cells to the treatment (cytotoxicity) can be determined by monitoring the total host-cell number. Therefore, multiple parameters on a cell-by-cell basis can be evaluated simultaneously in a single experiment and all captured images are stored automatically and can be reanalyzed later in time in order to extract meaningful quantitative data. In addition, its intuitive information content, the ability to visually confirm the data within the captured images, as well as its easy adaptability to 384 well-plates or higher throughput formats makes the assay particularly useful for screening applications. This assay might be especially useful for a wide range of applications in Chagas disease research, from small-molecule drug screening and inhibitor discovery to pathway elucidation.

Acknowledgments

This work was supported by NIH grants RO1AI070655, SO6GM00812, 2G12RR008124-16A1, and 2G12RR008124-16A1S1. Lilian L. Nohara was partially supported by the Cotton Memorial Scholarship (UTEP), Good Neighbor Scholarship (UTEP) and Florence Terry Griswold Scholarship-I (PARTT). The Cell Culture and High Throughput Screening (HTS), Biomolecule Analysis (BACF), and the Statistical Consulting Laboratory Core Facilities were supported by grants 5G12RR008124-16A1 (all Cores) and 2G12RR008124-16A1S1 (only BACF) to the Border Biomedical Research Center (BBRC), University of Texas at El Paso, from the National Center for Research Resources (NCRR), NIH.

References

1. Chagas C. Nova tripanosomiase humana. Estudos sobre a morfolojia e o ciclo evolutivo do *Schizotrypanum cruzi*, n.g., n. Sp., ajente etiolójico de nova entidade morbida do homem. Mem Inst Oswaldo Cruz 1909;1:159–218.
2. Schmunis GA. Epidemiology of Chagas disease in non-endemic countries: the role of international migration. Mem Inst Oswaldo Cruz 2007;102 Suppl 1:75–85. [PubMed: 17891282]
3. Bern C, Montgomery SP. An estimate of the burden of Chagas disease in the United States. Clin Infect Dis 2009;49:e52–e54. [PubMed: 19640226]
4. Bradley KK, Bergman DK, Woods JP, Crutcher JM, Kirchhoff LV. Prevalence of American trypanosomiasis (Chagas disease) among dogs in Oklahoma. J Am Vet Med Assoc 2000;217:1853–1857. [PubMed: 11132891]
5. Pung OJ, Banks CW, Jones DN, Krissinger MW. Trypanosoma cruzi in wild raccoons, opossums, and triatomine bugs in southeast Georgia, U.S.A. J Parasitol 1995;81:324–326. [PubMed: 7707220]
6. Reisenman CE, Lawrence G, Guerenstein PG, Gregory T, Dotson E, Hildebrand JG. Infection of kissing bugs with Trypanosoma cruzi, Tucson, Arizona, USA. Emerg Infect Dis 2010;16:400–405. [PubMed: 20202413]
7. Herwaldt BL, Grijalva MJ, Newsome AL, McGhee CR, Powell MR, Nemec DG, Steurer FJ, Eberhard ML. Use of polymerase chain reaction to diagnose the fifth reported US case of autochthonous transmission of Trypanosoma cruzi, in Tennessee, 1998. J Infect Dis 2000;181:395–399. [PubMed: 10608796]
8. Bern C, Montgomery SP, Katz L, Caglioti S, Stramer SL. Chagas disease and the US blood supply. Curr Opin Infect Dis 2008;21:476–482. [PubMed: 18725796]
9. Bowling J, Walter EA. Recognizing and meeting the challenge of Chagas disease in the USA. Expert Rev Anti Infect Ther 2009;7:1223–1234. [PubMed: 19968514]
10. Lauria-Pires L, Braga MS, Vexenat AC, Nitz N, Simoes-Barbosa A, Tinoco DL, Teixeira AR. Progressive chronic Chagas heart disease ten years after treatment with anti-Trypanosoma cruzi nitroderivatives. Am J Trop Med Hyg 2000;63:111–118. [PubMed: 11388500]
11. Croft SL, Barrett MP, Urbina JA. Chemotherapy of trypanosomiases and leishmaniasis. Trends Parasitol 2005;21:508–512. [PubMed: 16150644]

12. Tarleton RL, Reithinger R, Urbina JA, Kitron U, Gurtler RE. The challenges of Chagas Disease--grim outlook or glimmer of hope. PLoS Med 2007;4:e332. [PubMed: 18162039]
13. Rodriques Coura J, de Castro SL. A critical review on Chagas disease chemotherapy. Mem Inst Oswaldo Cruz 2002;97:3–24. [PubMed: 11992141]
14. Buckner FS, Wilson AJ, White TC, Van Voorhis WC. Induction of resistance to azole drugs in Trypanosoma cruzi. Antimicrob Agents Chemother 1998;42:3245–3250. [PubMed: 9835521]
15. Tyler KM, Engman DM. The life cycle of Trypanosoma cruzi revisited. Int J Parasitol 2001;31:472–481. [PubMed: 11334932]
16. Barrias ES, Reignault LC, De Souza W, Carvalho TM. Dynasore, a dynamin inhibitor, inhibits Trypanosoma cruzi entry into peritoneal macrophages. PLoS One 2010;5:e7764. [PubMed: 20098746]
17. Hoff R. Killing in vitro of Trypanosoma cruzi by macrophages from mice immunized with T. cruzi or BCG, and absence of cross-immunity on challege in vivo. J Exp Med 1975;142:299–311. [PubMed: 806649]
18. Woolsey AM, Burleigh BA. Host cell actin polymerization is required for cellular retention of Trypanosoma cruzi and early association with endosomal/lysosomal compartments. Cell Microbiol 2004;6:829–838. [PubMed: 15272864]
19. Andrade LO, Andrews NW. Lysosomal fusion is essential for the retention of Trypanosoma cruzi inside host cells. J Exp Med 2004;200:1135–1143. [PubMed: 15520245]
20. Rowland EC, Moore-Lai D, Seed JR, Stephens CE, Boykin DW. Inhibition of in vitro intracellular growth of Trypanosoma cruzi by dicationic compounds. J Parasitol 2003;89:1078–1080. [PubMed: 14627166]
21. Buckner FS, Verlinde CL, La Flamme AC, Van Voorhis WC. Efficient technique for screening drugs for activity against Trypanosoma cruzi using parasites expressing beta-galactosidase. Antimicrob Agents Chemother 1996;40:2592–2597. [PubMed: 8913471]
22. Yan W, Moreno SN. A method to assess invasion and intracellular replication of Trypanosoma cruzi based on differential uracil incorporation. J Immunol Methods 1998;220:123–128. [PubMed: 9839933]
23. Hyland KV, Asfaw SH, Olson CL, Daniels MD, Engman DM. Bioluminescent imaging of Trypanosoma cruzi infection. Int J Parasitol 2008;38:1391–1400. [PubMed: 18511053]
24. Mezencev R, Galizzi M, Kutschy P, Docampo R. Trypanosoma cruzi: antiproliferative effect of indole phytoalexins on intracellular amastigotes in vitro. Exp Parasitol 2009;122:66–69. [PubMed: 19545522]
25. Kraus JM, Verlinde CL, Karimi M, Lepesheva GI, Gelb MH, Buckner FS. Rational modification of a candidate cancer drug for use against Chagas disease. J Med Chem 2009;52:1639–1647. [PubMed: 19239254]
26. Zanella F, Lorens JB, Link W. High content screening: seeing is believing. Trends Biotechnol. 2010
27. Link W, Oyarzabal J, Serelde BG, Albarran MI, Rabal O, Cebria A, Alfonso P, Fominaya J, Renner O, Peregrina S, Soilan D, Ceballos PA, Hernandez AI, Lorenzo M, Pevarello P, Granda TG, Kurz G, Carnero A, Bischoff JR. Chemical interrogation of FOXO3a nuclear translocation identifies potent and selective inhibitors of phosphoinositide 3-kinases. J Biol Chem 2009;284:28392–28400. [PubMed: 19690175]
28. Agler M, Prack M, Zhu Y, Kolb J, Nowak K, Ryseck R, Shen D, Cvijic ME, Somerville J, Nadler S, Chen T. A high-content glucocorticoid receptor translocation assay for compound mechanism-of-action evaluation. J Biomol Screen 2007;12:1029–1041. [PubMed: 17989426]
29. Ross DA, Lee S, Reiser V, Xue J, Alves K, Vaidya S, Kreamer A, Mull R, Hudak E, Hare T, Detmers PA, Lingham R, Ferrer M, Strulovici B, Santini F. Multiplexed assays by high-content imaging for assessment of GPCR activity. J Biomol Screen 2008;13:449–455. [PubMed: 18519922]
30. De Rycker M, Rigoreau L, Dowding S, Parker PJ. A high-content, cell-based screen identifies micropolyin, a new inhibitor of microtubule dynamics. Chem Biol Drug Des 2009;73:599–610. [PubMed: 19635051]
31. Conrad C, Gerlich DW. Automated microscopy for high-content RNAi screening. J Cell Biol 2010;188:453–461. [PubMed: 20176920]

32. Kuijl C, Savage ND, Marsman M, Tuin AW, Janssen L, Egan DA, Ketema M, van den Nieuwendijk R, van den Eeden SJ, Geluk A, Poot A, van der Marel G, Beijersbergen RL, Overkleeft H, Ottenhoff TH, Neefjes J. Intracellular bacterial growth is controlled by a kinase network around PKB/AKT1. Nature 2007;450:725–730. [PubMed: 18046412]

33. Engel JC, Ang KK, Chen S, Arkin MR, McKerrow JH, Doyle PS. Image-Based High Throughput Drug Screening Targeting the Intracellular Stage of Trypanosoma cruzi, the Agent of Chagas' Disease. Antimicrob Agents Chemother. 2010

34. Andrews NW, Colli W. Adhesion and interiorization of Trypanosoma cruzi in mammalian cells. J Protozool 1982;29:264–269. [PubMed: 7047731]

35. Uphoff CC, Drexler HG. Detection of mycoplasma contaminations. Methods Mol Biol 2005;290:13–23. [PubMed: 15361652]

36. Burleigh BA, Woolsey AM. Cell signalling and Trypanosoma cruzi invasion. Cell Microbiol 2002;4:701–711. [PubMed: 12427093]

37. Andrade LO, Andrews NW. The Trypanosoma cruzi-host-cell interplay: location, invasion, retention. Nat Rev Microbiol 2005;3:819–823. [PubMed: 16175174]

38. Ley V, Andrews NW, Robbins ES, Nussenzweig V. Amastigotes of Trypanosoma cruzi sustain an infective cycle in mammalian cells. J Exp Med 1988;168:649–659. [PubMed: 3045248]

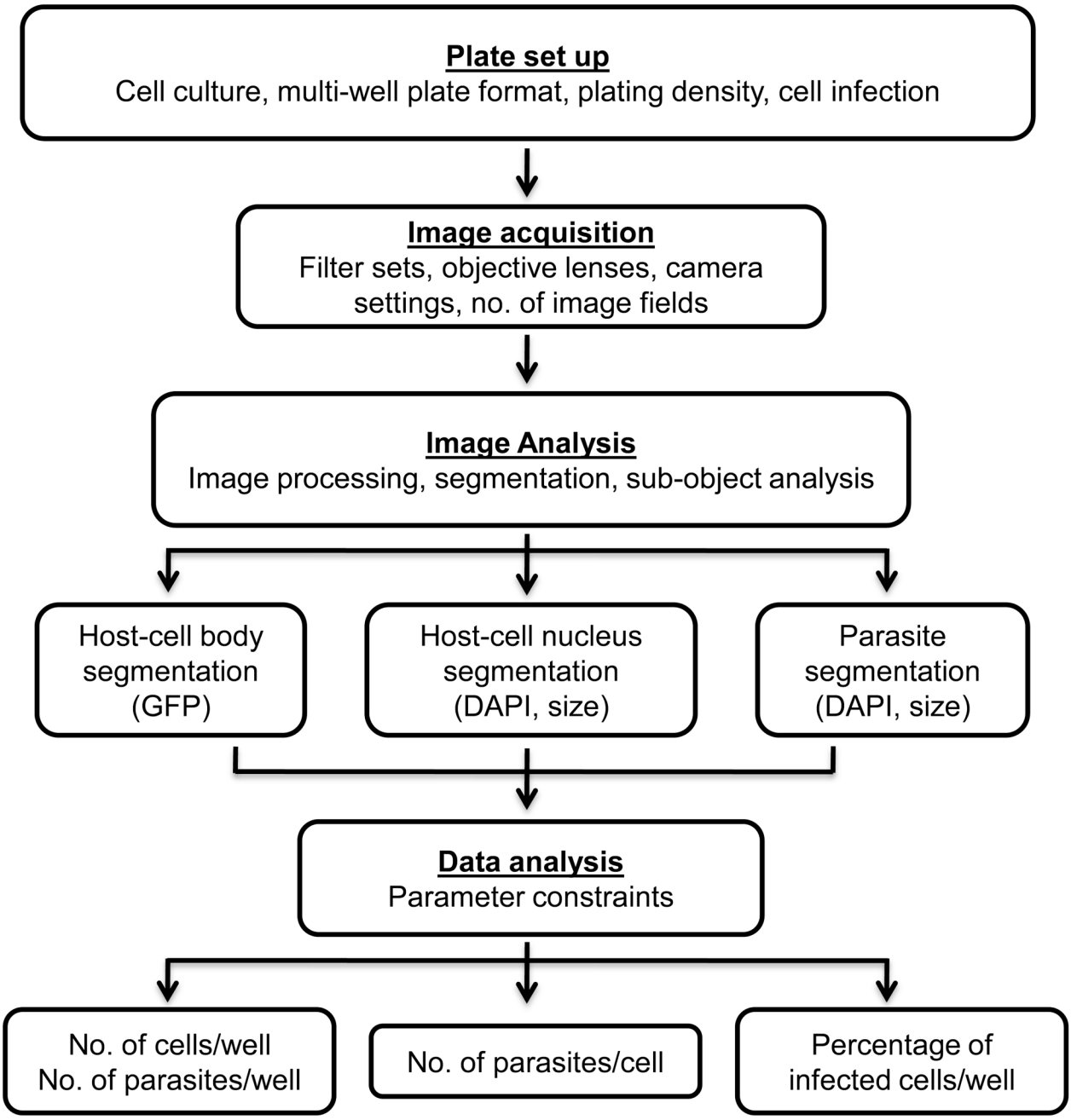

Figure 1.

General workflow of high-content imaging applied for automated analysis of infection rate by *T. cruzi*. A high-resolution fluorescence bioimager system was applied for image acquisition, data processing, and analysis of *T. cruzi*-infected, GFP-expressing NIH3T3 cells, in a 96-well plate format. Images of GFP fluorescence (host cell) and DAPI (host-cell and parasite DNA) from nine contiguous image fields (3 × 3 montage) were acquired per well with a 20× 0.75 NA objective. For optimal segmentation and accurate quantification several image processing and segmentation tools were combined in order to optimize the image analysis protocol. GFP was used to define the host-cell body (boundary object), whereas DAPI was used to define the

intracellular parasites (sub-object) and the host-cell nuclei. Numerical data was used for the analysis of multiparametric data associated with infection of host cells by *T. cruzi*.

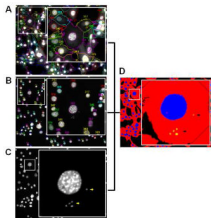

Figure 2.

Representative cropped, segmented images (20×, 0.75 NA) of GFP-expressing NIH 3T3 cells infected with *T. cruzi*. **A.** Host-cell body segmentation based on GFP expression. **B.** Host-cell nucleus segmentation based on DAPI staining. **C.** *T. cruzi* segmentation based on DAPI staining of parasite nuclear and kinetoplast DNA, and size threshold. Yellow arrows denote parasite DNA. **D.** Segmentation mask of the same image generated after sub-object analysis depicting host-cell bodies (red), host-cell nuclei (blue), and parasites (yellow). Small numbers in **A** and **B** denote host-cell bodies and nuclei, respectively. Insets in **A–D** indicate higher magnification of areas delimited by white squares within the main images.

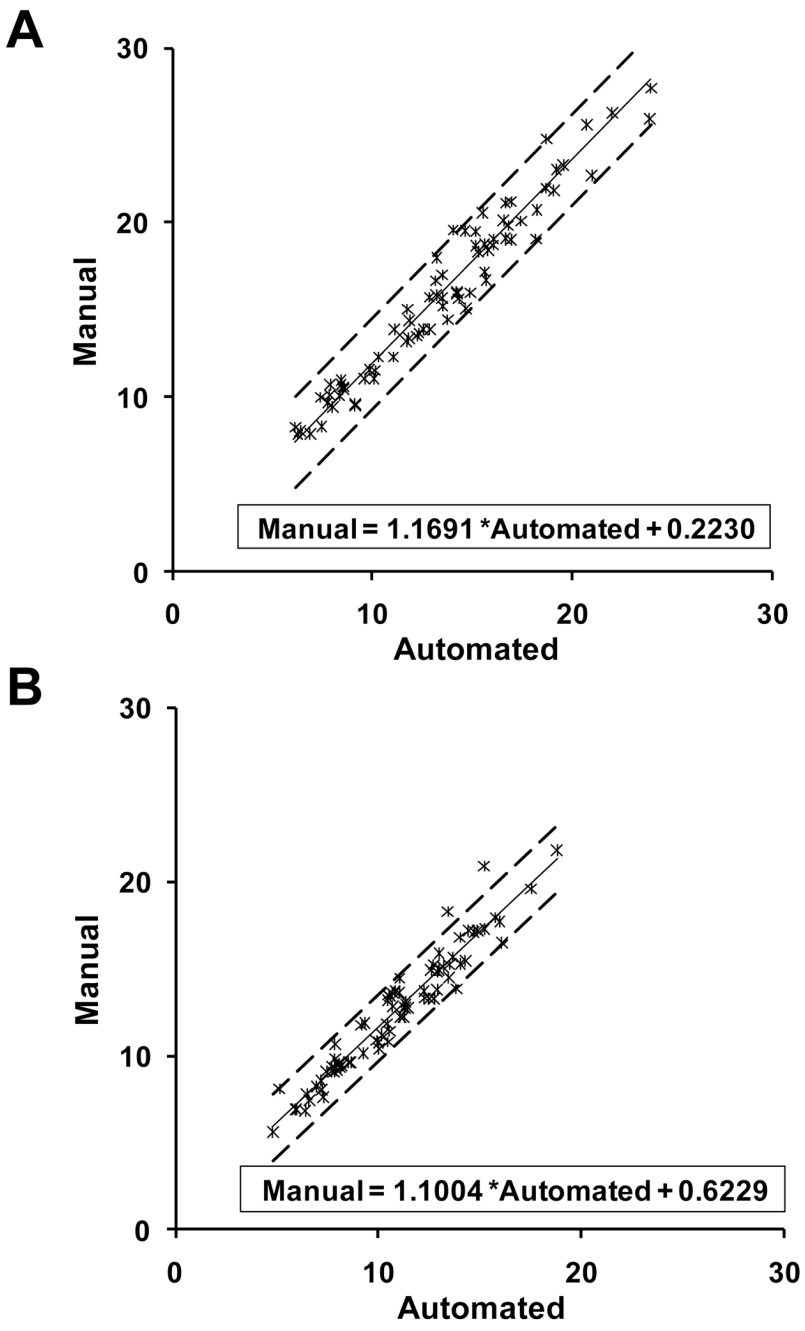

Figure 3.

Scatter plots of manual versus automated intracellular *T. cruzi* counting methods. **A.** Scatter plot comparing manual versus automated method for counting the number of parasites per 100 cells with the fitted regression line and the 95% confidence bounds for individual values. **B.** Scatter plot comparing manual versus automated method for determining the percentage of infected cells with the fitted regression line and the 95% confidence bounds for individual values. In both plots, the scatter about the fitted regression line is quite small and the slope of the line is positive (small manual values correspond to small automated values; large manual values correspond to large automated values), thus indicating a positive correlation between manual and automated methods.

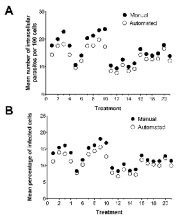

Figure 4.
Comparison of data point means between manual and automated *T. cruzi* counting methods. **A.** Mean number of parasites per 100 cells, by treatment and method. **B.** Mean percentage of infected cells, by treatment and method.

Table 1

Statistics summary for the absolute difference and the percent absolute difference between the manual and automated intracellular *T. cruzi* counting methods

Parameter	Variable	N	Mean	SD[a]
Number of parasites per 100 cells	Absolute difference	77	2.5	1.5
	Percent absolute difference	77	15.4	6.3
Percentage of infected cells	Absolute difference	77	1.7	1.0
	Percent absolute difference	77	13.6	6.3

[a]Standard deviation

Table 2

Estimated time required to process a 96-well plate by the manual and automated methods

Method	Step	Duration (h)	Total (h)	Working hours [a]	Working days [b]
Manual	Visual counting and manual scoring	96	96	96	12
Automated	Image capture	1.5	14	≈ 2	≈ 2
	Image analysis	12			
	Data analysis	0.5			

[a] Working hours used by the operator to perform the method

[b] A working day is defined as an 8-h day.

≈ Approximately equal to